Available online at www.sciencedirect.com
ScienceDirect
European Journal of Mechanics B/Fluids 26 (2007) 669–687

Numerical simulation of unsteady mixed convection in a driven cavity using an externally excited sliding lid

Khalil M. Khanafer [a], Abdalla M. Al-Amiri [b], Ioan Pop [c,*]

[a] *Biomedical Engineering Department, University of Michigan, Ann Arbor, MI 48109, USA*
[b] *Mechanical Engineering Department, United Arab Emirates University, P.O. Box 17555 Al-Ain, United Arab Emirates*
[c] *Faculty of Mathematics, University of Cluj, R-3400 Cluj, Romania*

Received 18 October 2005; received in revised form 20 April 2006; accepted 22 June 2006

Available online 3 March 2007

Abstract

A numerical investigation of unsteady laminar mixed convection heat transfer in a lid driven cavity is executed. The forced convective flow inside the cavity is attained by a mechanically induced sliding lid, which is set to oscillate horizontally in a sinusoidal fashion. The natural convection effect is sustained by subjecting the bottom wall to a higher temperature than its top counterpart. In addition, the two vertical walls of the enclosure are kept insulated. Discretization of the governing equations is achieved through a finite element scheme based on the Galerkin method of weighted residuals. Comparisons with previously reported investigations are performed and the results show excellent agreement. Temporal variations of streamlines, isotherms, and dimensionless drag force, and Nusselt number are presented in this investigation for various pertinent dimensionless groups. Fluid flow and heat transfer characteristics are examined in the domain of the Reynolds number, Grashof number and the dimensionless lid oscillation frequency such that: $10^2 \leqslant Re \leqslant 10^3$, $10^2 \leqslant Gr \leqslant 10^5$ and $0.1 \leqslant \varpi \leqslant 5$. The working fluid is assigned a Prandtl number of 0.71 throughout this investigation. The obtained results reveal that the Reynolds number and Grashof number would either enhance or retard the energy transport process and drag force behavior depending on the conduct of the velocity cycle. Moreover, relatively small lid oscillation values are found to constrain the lid associated motion to a shallow depth from the sliding lid plane.

Keywords: Cavity; Mixed convection; Numerical; Sliding lid; Unsteady

1. Introduction

The fundamental problem of combined forced and natural convection heat transfer in a closed cavity has received considerable attention from researchers. Such a problem is customary grouped under the lid driven cavity problems. This problem is often encountered in industrial processes and in nature. The modeling and simulation of crystal growth, glass production, food processing, nuclear reactors and food processing are common examples of current industrial applications while convective thermal currents associated with the flow structure occurring in lakes and reservoirs are typically cited as a natural phenomenon.

* Corresponding author.
E-mail addresses: khanafer@umich.edu (K.M. Khanafer), alamiri@uaeu.ac.ae (A.M. Al-Amiri), popi@math.ubbcluj.ro (I. Pop).

0997-7546/$ – see front matter
doi:10.1016/j.euromechflu.2006.06.006

Nomenclature

D	dimensionless average drag force
g	gravitational acceleration ..... $\mathrm{m\,s^{-2}}$
Gr	Grashof Number $= g\beta\Delta T H^3/\nu^2$
H	cavity height ..... m
n	Newton iteration index
$\overline{Nu}$	average Nusselt number
P	dimensionless fluid pressure $= pH/(\rho\nu u_0)$
Pr	Prandtl number $= \nu/\alpha$
Re	Reynolds number $= u_0 H/\nu$
Ri	Richardson number $= Gr/Re^2$
T	temperature ..... °C
ΔT	temperature difference $= T_{\mathrm{hot}} - T_{\mathrm{cold}}$ .. °C
t	time ..... s
u	velocity in x-direction ..... $\mathrm{m\,s^{-1}}$
u_0	maximum lid speed ..... $\mathrm{m\,s^{-1}}$
U	dimensionless horizontal velocity $= u/u_0$
v	velocity in y-direction ..... $\mathrm{m\,s^{-1}}$
V	dimensionless vertical velocity $= v/u_0$
x, y	Cartesian coordinates ..... m
X, Y	dimensionless Cartesian coordinates $= (x, y)/H$

Greek symbols

α	thermal diffusivity of the fluid ..... $\mathrm{m^2\,s^{-1}}$
β	coefficient of thermal expansion of fluid ..... $\mathrm{K^{-1}}$
λ	period of oscillation $= 2\pi/\varpi$ ..... s
ν	kinematic viscosity ..... $\mathrm{m^2\,s^{-1}}$
θ	dimensionless temperature $= (T - T_{\mathrm{cold}})/\Delta T$
ω	lid oscillation frequency ..... $\mathrm{rad\,s^{-1}}$
ϖ	dimensionless lid frequency $= \omega H/u_0$
ρ	fluid density ..... $\mathrm{kg\,m^{-3}}$
τ	dimensionless time $= tu_0/H$

Subscript

cold	cold wall
hot	hot wall

Understanding the fundamental knowledge about the pertinent transport processes and the operational parameters are the key to provide sound insight into this problem. The physically inherited characteristics of this class of problems have been extensively explored in the literature [1–5]. In addition, Moallemi and Jang [6] studied the effect of Prandtl number and Reynolds number on the flow and thermal characteristics of a laminar mixed convection in a rectangular cavity. Furthermore, Iwatsu et al. [7] have conducted a numerical investigation of a two-dimensional driven-cavity flow under the steady state condition with a vertical temperature gradient. They have produced similar patterns to mixed convection flows when incorporating small Richardson number values. Giving the popularity of the lid-driven cavity problem, it is also widely used as a benchmark tool for the appraisal of different numerical schemes [8–11]. The non-linear dependency of liquids density on temperature has also received considerable attention since such a scenario tends to complicate the structure of the convective flows considerably [12]. Prasad and Koseff [13] have reported experimental results on mixed convection heat transfer process in a lid-driven cavity for a range of Richardson number between 0.1 and 1000. They have concluded that the heat transfer mechanism is a weak function of the Richardson number as compared to the considered Reynolds number and physical aspect ratio values.

On the contrary, the effect of an external oscillating sliding lid in driven cavity flows has received little research attention although it is important for understanding the transport phenomena in food processing applications, for example. Soh and Goodrich [14] outlined the basic transient flow features relevant to this problem using a time-accurate finite-difference scheme. Moreover, Iwatsu et al. [15] performed a numerical investigation on the effect of external excitation on the flow structure in a square cavity. Their results have shown similar flow structure to steady driven-cavity flows when utilizing small frequency values. Such a similarity, however, was noted to vanish when large frequency values were employed. A subsequent work by Iwatsu et al. [16] carried out a numerical study of the viscous flow in a heated driven-cavity under thermal stratification, where the oscillating lid was maintained at a higher temperature than the lower wall. Their results had revealed substantial enhancement in heat transfer rate at particular lid frequency values, which signals the presence of the resonance phenomena. From the above discussion and the survey of literature, it seems that the problem of mixed convection heat transfer in a cavity heated from below subjected to a sliding lid that exercises a mechanical oscillation has not been addressed yet. Such studies have been limited as discussed above to driven cavities under thermal stratification condition.

Hence, the main objective of the present investigation is to examine the flow and heat transfer characteristics of an unsteady laminar mixed convection heat transfer in a cavity heated from below with a moving lid that exercises

oscillations in the horizontal plane. The consequences of varying the Reynolds number, Grashof number, and the lid oscillation frequency on the transport processes will be highlighted and discussed. In addition, the temporal variation of the average Nusselt number and the dimensionless drag force will be documented for the considered case studies.

2. Mathematical formulation

A two-dimensional square cavity is considered for the present study with the physical dimensions given in Fig. 1. The horizontal walls of the cavity are maintained at uniform but different temperature values. In fact, the bottom wall is sustained at a higher temperature to induce buoyancy effect. In addition, the vertical walls are assumed adiabatic. The mechanically induced lid motion is assumed to oscillate with a velocity $u = u_0 \sin \omega t$ in the longitudinal direction, where u_0 is the maximum oscillating speed of the lid and ω is the oscillating frequency. The no-slip condition is imposed at the solid walls. The working fluid is assumed to be an incompressible Newtonian fluid and is considered to operate under the laminar regime. Furthermore, the thermophysical properties are assumed constant except for the density in the buoyancy force, which is assumed to have a linear dependency on temperature according to Boussinesq formulation.

Based on the above considerations, the following dimensionless variables are introduced

$$X = \frac{x}{H}, \quad Y = \frac{y}{H}, \quad U = \frac{u}{u_0}, \quad V = \frac{\upsilon}{u_0},$$
$$\tau = \frac{u_0 t}{H}, \quad \varpi = \frac{\omega H}{u_0}, \quad \theta = \frac{T - T_{\text{cold}}}{\Delta T}, \quad P = \frac{pH}{\rho \nu u_0},$$
$$Re = \frac{u_0 H}{\nu}, \quad Gr = \frac{g\beta \Delta T H^3}{\nu^2}, \quad Pr = \frac{\nu}{\alpha} \tag{1}$$

where $\Delta T = T_{\text{hot}} - T_{\text{cold}}$, P is the dimensionless pressure, Re is the Reynolds number, Gr is the Grashof number and Pr is the Prandtl number.

According to the above assumptions and dimensionless variables, the normalized governing equations are expressed in the following format

$$\frac{\partial U}{\partial X} + \frac{\partial V}{\partial Y} = 0, \tag{2}$$
$$\frac{\partial U}{\partial \tau} + U\frac{\partial U}{\partial X} + V\frac{\partial U}{\partial Y} = \frac{1}{Re}\left(-\frac{\partial P}{\partial X} + \nabla^2 U\right), \tag{3}$$
$$\frac{\partial V}{\partial \tau} + U\frac{\partial V}{\partial X} + V\frac{\partial V}{\partial Y} = \frac{1}{Re}\left(-\frac{\partial P}{\partial Y} + \nabla^2 V + \frac{Gr}{Re}\theta\right), \tag{4}$$

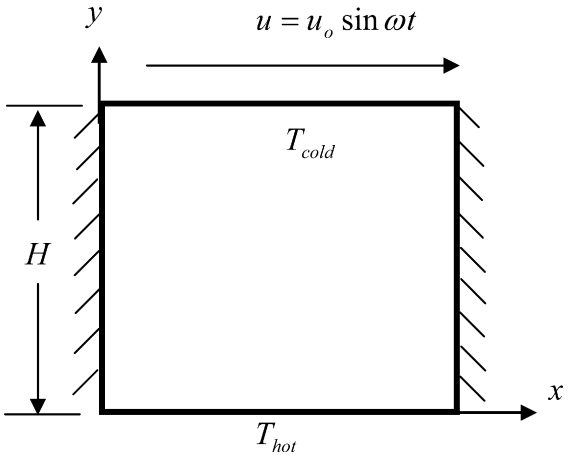

Fig. 1. A schematic diagram of the physical model.

$$\frac{\partial\theta}{\partial\tau} + U\frac{\partial\theta}{\partial X} + V\frac{\partial\theta}{\partial Y} = \frac{\nabla^2\theta}{PrRe}. \tag{5}$$

For $\tau > 0$, the steady state solution for temperature and flow velocity fields of a lid moving at a constant speed (i.e., $U = 1$) is used as an initial condition for the torsionally-oscillating lid in this investigation. Meanwhile, the dimensionless boundary conditions used are summarized as follows

$$\begin{aligned} &U = V = 0, \quad \frac{\partial\theta}{\partial X} = 0, && X = 0, 1;\ 0 \leqslant Y \leqslant 1, \\ &U = V = 0, \quad \theta = 1, && Y = 0,\ 0 < X < 1, \\ &U = \sin\varpi\tau, \quad V = 0,\ \theta = 0, && Y = 1,\ 0 < X < 1. \end{aligned} \tag{6}$$

The time history of the dimensionless heat flux is computed through calculating the average Nusselt number along both the top and bottom walls using

$$\overline{Nu} = -\int_0^1 \frac{\partial\theta}{\partial Y}\,\mathrm{d}X. \tag{7}$$

Also, the chronicle development of the dimensionless drag force exerted on the oscillating lid is given by

$$D = \int_0^1 \frac{\partial U}{\partial Y}\,\mathrm{d}X. \tag{8}$$

It should be pointed out that the singularities in axial U velocity at the two upper corners are treated using a similar approach as reported in Refs. [17–19].

3. Solution method

The solution of the governing equations along with the initial and boundary conditions are solved through the Galerkin finite element formulation. An implicit scheme is employed to deal with the time differential terms. The continuum domain is divided into a set of non-overlapping regions called elements. Nine node quadrilateral elements with bi-quadratic interpolation functions are utilized to discretize the physical domain. Moreover, interpolation functions in terms of local normalized element coordinates are employed to approximate the dependent variables within each element. Substitution of the obtained approximations into the system of the governing equations and boundary conditions yields a residual for each of the conservation equations. These residuals are reduced to zero in a weighted sense over each element volume using the Galerkin method.

The pressure term in the momentum equations is manipulated using the consistent penalty model [17]. In addition, the non-linear terms in the momentum equations are manipulated using the Newton–Raphson iteration algorithm. The velocity and temperature terms are expressed as quadrilateral and nine-node quadratic isoparametric elements. The application of this technique and the discretization procedures are well documented by Taylor and Hood [18] and Gresho et al. [19]. Extensive numerical experimentations are performed to eliminate mesh sensitivity for the considered field variables. The convergence of solutions is assumed when the relative error for each variable between consecutive iterations is recorded below the convergence criterion ε such that

$$\left|\frac{\Gamma^{n+1} - \Gamma^n}{\Gamma^{n+1}}\right|_{\tau+\Delta\tau} < \varepsilon \tag{9}$$

where n is the Newton iteration index and $\Gamma = U, V, \theta$. The convergence criterion was set to 10^{-4}.

4. Algorithm validation

A variable mesh size system of (81×81) is implemented in the present investigation with finer mesh sizes being deployed near the cavity walls to capture the rapid changes in the structure of the dependent variables. The verification of the current algorithm is carried out in two folds. First, the present numerical solution is verified against

Table 1
Comparison of the limits of velocity components between the present solution and other solutions at $Gr = 10^2$

Parameter	$Re = 100$			$Re = 1000$	
	Present	Ref. [19]	Ref. [20]	Present	Ref. [19]
U_{min}	−0.2093	−0.2037	−0.2122	−0.3718	−0.3782
U_{max}	1.0	1.0	1.0	1.0	1.0
V_{min}	−0.2482	−0.2448	−0.2506	−0.5038	−0.5178
V_{max}	0.1720	0.1699	0.1765	0.3588	0.3658

Table 2
Comparison of the average Nusselt number at the top wall between the present solution and other solutions

Parameter	$Gr = 10^2$			$Gr = 10^6$	
	Present	Ref. [19]	Ref. [20]	Present	Ref. [19]
$Re = 100$	2.02	1.94	2.01	1.02	1.02
$Re = 400$	4.01	3.84	3.91	1.17	1.22
$Re = 1000$	6.42	6.33	6.33	1.72	1.77

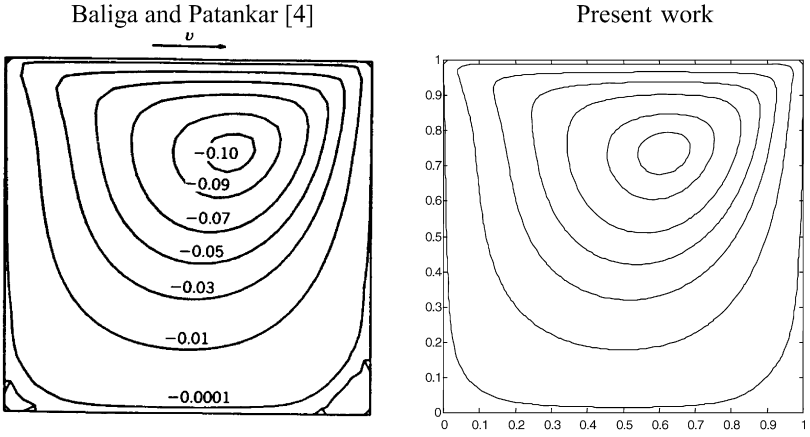

Fig. 2. Comparison of the Driven-cavity stream function between the present work and Baliga and Patankar [4] for $Re = 100$.

two documented numerical studies. Namely, the numerical solutions reported by Iwatsu et al. [7] and Al-Amiri [20], which is based on a finite volume scheme. The findings of the comparisons are documented in Tables 1 and 2 for the bounds on the magnitudes of the velocity components and the average Nusselt number predictions, respectively. Both comparisons illustrate close proximity in the predictions made between the various solutions.

The second fold is a comparison between the predicted stream function contours under steady state condition of the present work to that of Baliga and Patankar [4]. As displayed in Fig. 2, the comparison strikes an excellent agreement between both studies. Further validation case studies are documented in Al-Amiri and Khanafer [21]. These validation cases boost the confidence in the numerical outcome of the present work.

5. Results and discussion

As stated earlier, the overall objective of the current investigation is to explore time dependent laminar mixed convection heat transfer in a lid-driven cavity. The implications of varying the Reynolds number, Grashof number and the lid oscillation frequency will be emphasized. The results are presented in terms of the temporal variation of the velocity and temperature profiles, streamline and isotherm patterns. What is more, the temporal variations of the average Nusselt number and drag force are highlighted. The Reynolds number is varied between 100 and 1000. In addition, the domain of Grashof number and dimensionless lid oscillation frequency is varied in the range of $10^2 \leqslant Gr \leqslant 10^5$ and $0.1 \leqslant \varpi \leqslant 5$, respectively.

5.1. Effect of Reynolds number on the temporal variation of the velocity and temperature profiles at the respective mid sections of the cavity

First, the effect of Reynolds number is studied while Gr and ϖ values were fixed at 100 and 1, respectively. The customary dimensional velocity components and (U, V) and temperature (θ) distributions for this class of cavity driven problems are typically plotted at the respective mid sections of the cavity. The temporal variation of the velocity and temperature profiles is presented for $Re = 100$ as shown in Fig. 3. The flow development in the cavity is controlled merely by the buoyancy force when $\tau = 0$. For positive lid velocity values $(0 < \tau < \pi)$, the mechanically induced shear force assists the horizontal velocity strength. In contrast, the lid velocity alters its sign once it enters the second half of the cycle $(\pi \leqslant \tau < 2\pi)$. Accordingly, the horizontal velocity component reverses its direction and, thus, looses much of its intensity in the vicinity of the lid region as it is faced with the counteract flow action sustained by the buoyancy force. The profile of the vertical velocity component indicates appreciated increase in the first half of the velocity cycle. The effect of the sidewalls appears to be significant for this case study.

It is noticed, however, that the flow activities in the bulk of the cavity tend to diminish in the second half of the velocity cycle. Although the shear force registered at $\tau = 1.5\pi$ appears to cause appreciated flow movement in the proximity of the lid, the bottom half of the cavity is close to a stagnant flow condition. Such an impact is vivid on the temperature profile, which assumes a linear profile with the increase of the oscillation period for a given time period. This signals the existence of a profound conduction heat transfer regime.

The increase of Reynolds number to 400, as shown in Fig. 4, brings about appreciated increase in the offered shear force and, subsequently, higher flow activities. Consequently, both velocity components register larger magnitudes in the bulk of the cavity. As a result, a greater flow penetration depth is achieved and the temperature profile is shown to depict significant convection heat transfer contribution to the overall energy transport process while conduction heat transfer regime becomes confined to the bottom twenty percent of the cavity.

5.2. Effect of Reynolds number on the temporal variation of the streamlines and isotherms

Fig. 5 illustrates the impact of Re on the temporal variation of the streamlines and isotherms for $Gr = 100$ and $\varpi = 1$. The intensity of flow activities for each time period was documented by recording the maximum and minimum streamline values. For a relatively small Reynolds number, i.e., $Re = 100$, Fig. 5(a) shows a primary vortex occupying much of the cavity for all the considered time periods. This implies that the fluid is well mixed. It is also noticed that the negative lid speed values cause the center of the vortex to move from right to left as the sliding lid switches directions. Furthermore, the streamline intensity level is weakened at this stage owing to the apparent opposing forces of shear and buoyancy, which impede downward flow penetration. As a result, the isotherms patterns become stratified except in the vicinity of the sliding lid.

When Re is set to 1000, as shown in Fig. 5(b), the flow circulation strengthens which facilitates augmentation of heat transfer process. This manifest that convection heat transfer has become the primary energy carrier in this case. In addition, the strength of the shear force offers a counteraction to the sustained buoyancy effect for negative lid speed as stated earlier. Due to the overwhelming effect of the existing shear force, the primary vortex is found to break up into two vortices filling much of the cavity. The isotherms are accordingly clustered close to the bottom wall, which points out to the existence of high temperature gradients in the vertical direction.

5.3. Effect of Reynolds number on the average Nusselt number and drag force

The effect of the Reynolds number on the predicted average Nusselt number and drag force is displayed in Fig. 6 for $Gr = 100$ and $\varpi = 1$. The results indicate that as the Reynolds number increases, the average Nusselt number predictions along the top and bottom walls shall increase as well. This is attributed to the high flow activities within the cavity. It is worth noting that the average Nusselt number along the bottom wall is almost constant which is attributed to the overwhelming effect of the sliding lid. The effect of the Reynolds number on the drag force acting on the sliding lid for various times is also shown in Fig. 6. It is observed that the drag force mimics the same sinusoidal behavior of the external excitation offered by the sliding lid. Furthermore, the drag force is found to increase with the increase in Re due to the rise in the viscous effect.

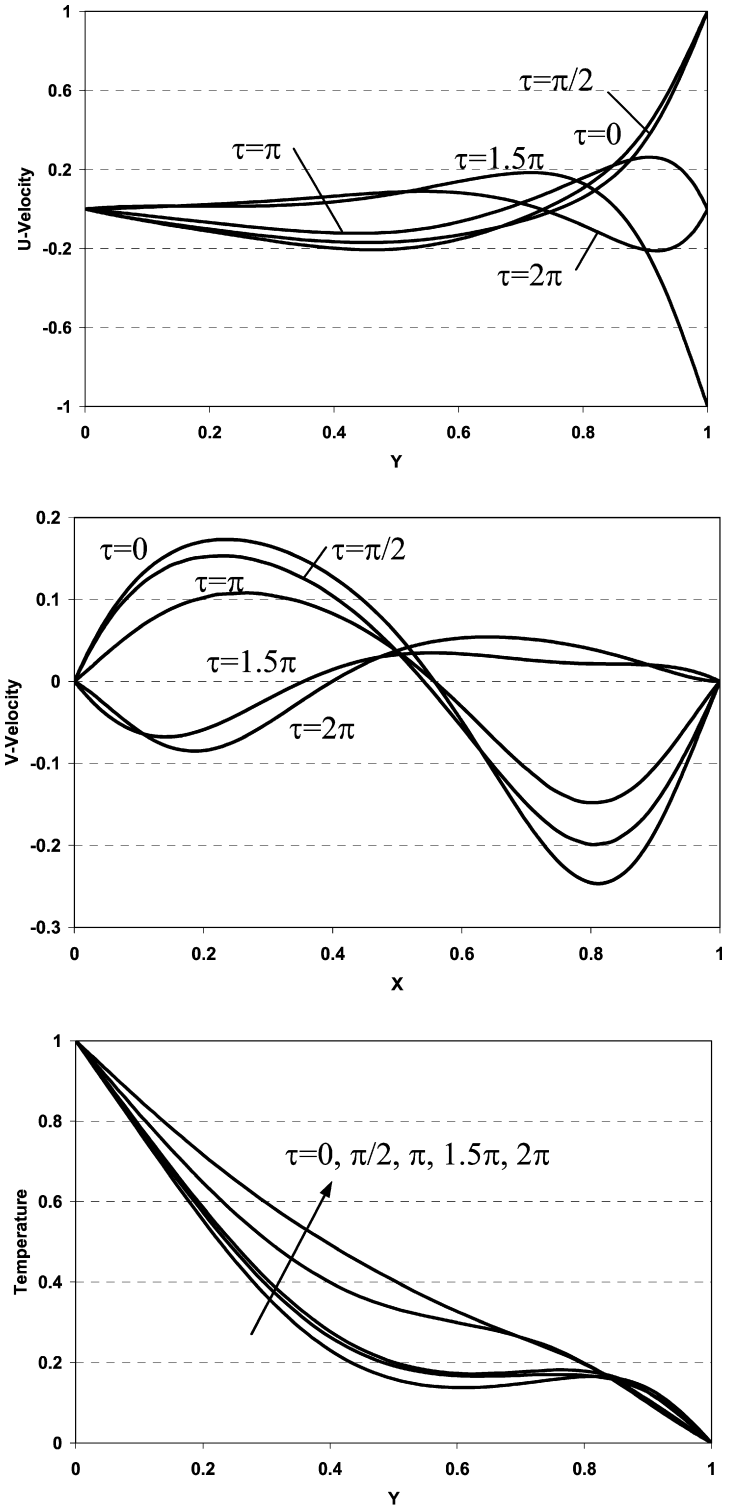

Fig. 3. Variation of the temperature and velocity profiles at the respective mid sections for $Re = 100$, $Gr = 100$ and $\varpi = 1$.

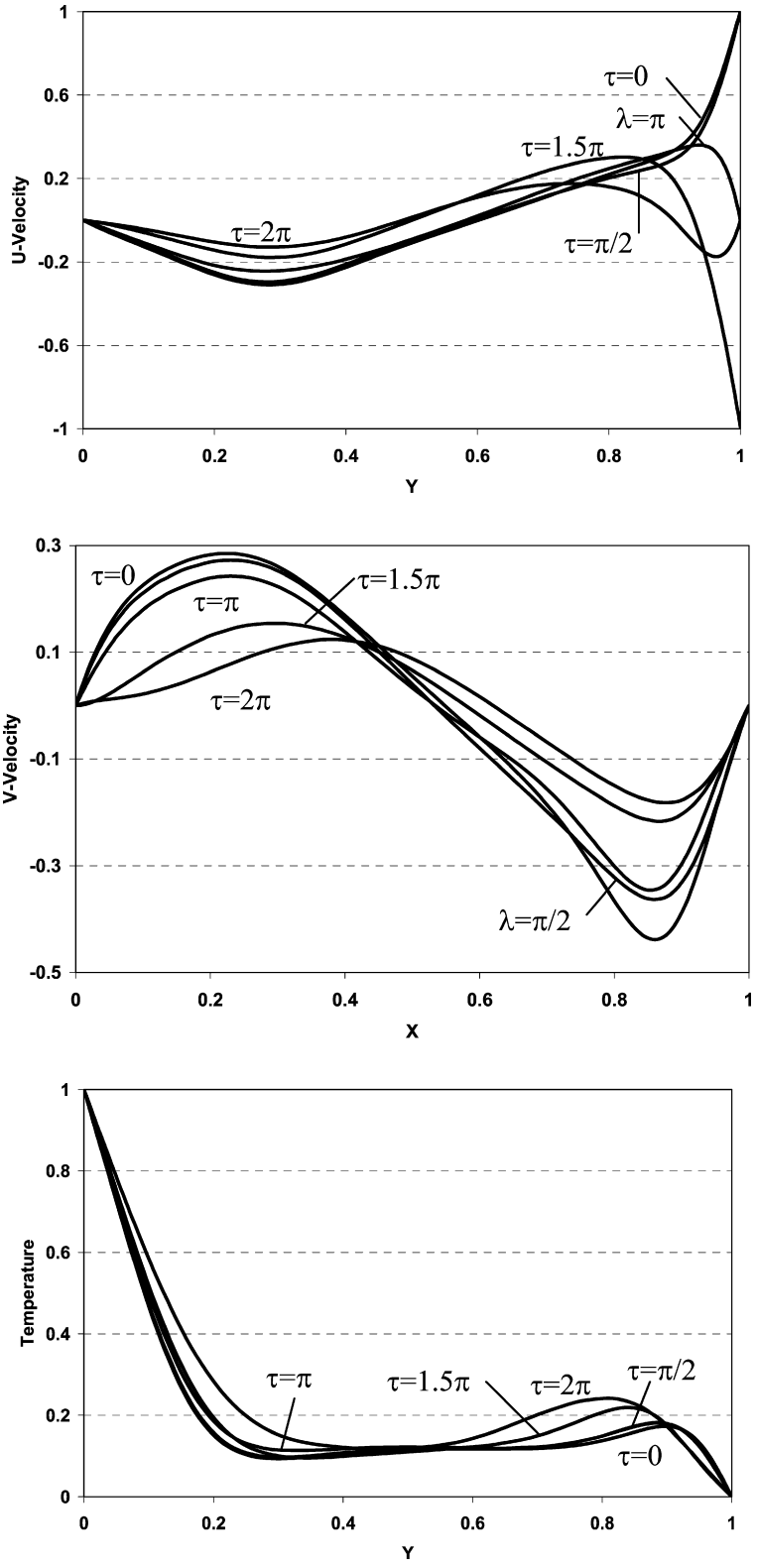

Fig. 4. Variation of the temperature and velocity profiles at the respective mid sections for $Re = 400$, $Gr = 100$ and $\varpi = 1$.

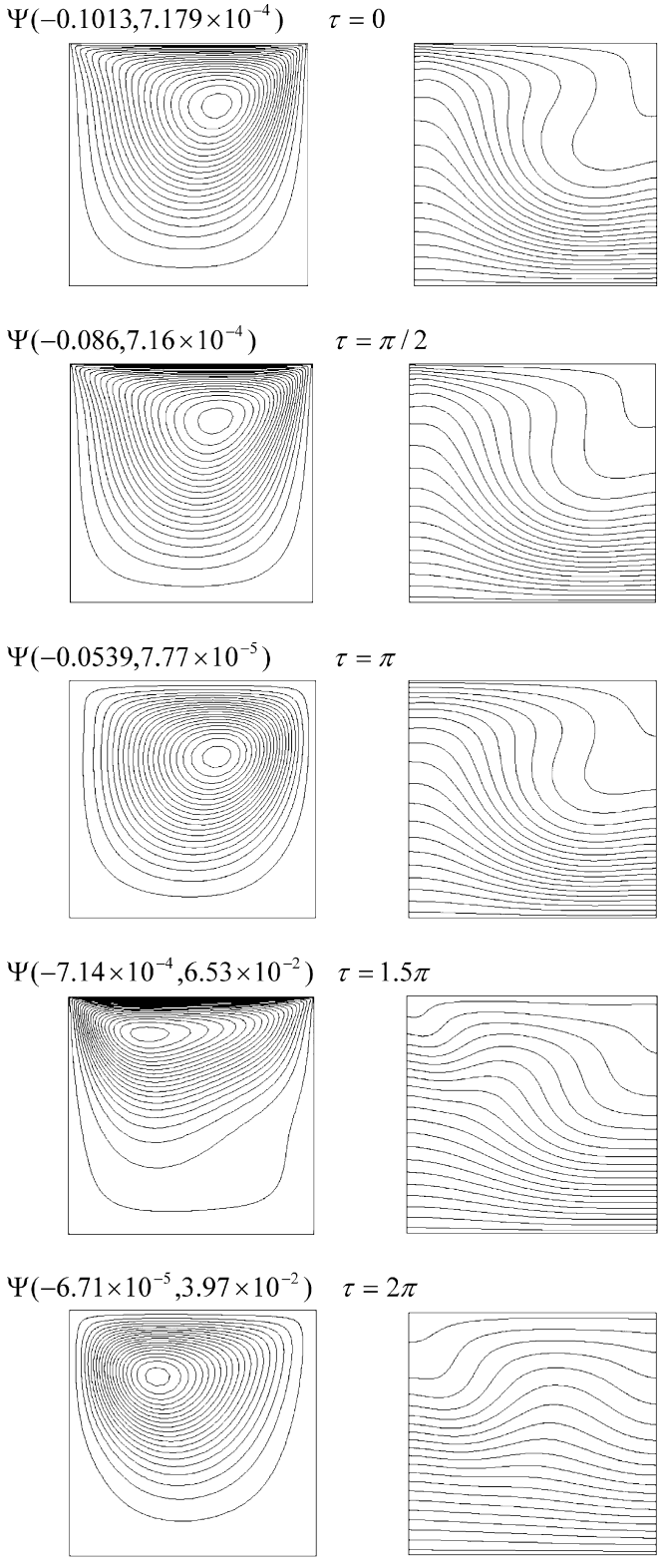

(a)

Fig. 5. (a) Variation of the streamline and isotherm contours for $Re = 100$, $Gr = 100$ and $\varpi = 1$. (b) Variation of the streamline and isotherm contours for $Re = 1000$, $Gr = 100$ and $\varpi = 1$.

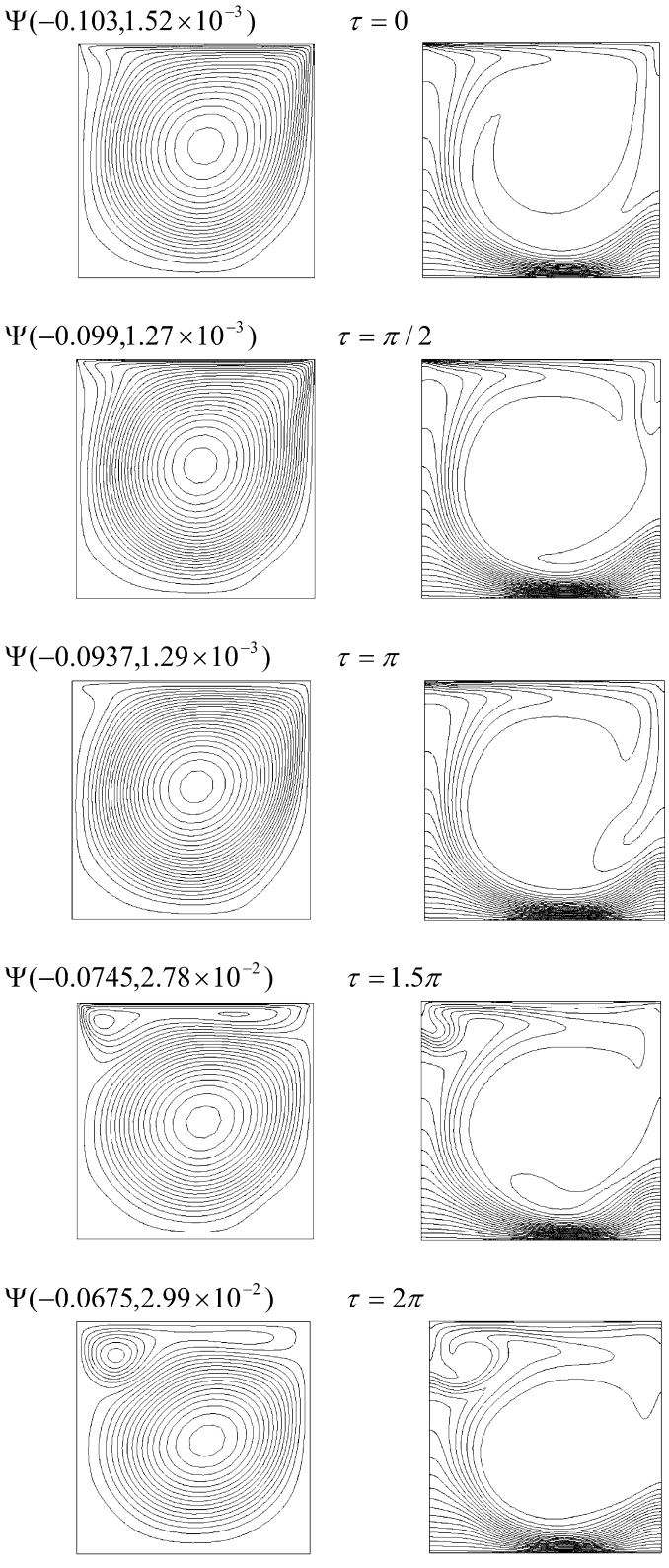

(b)

Fig. 5 (*continued*).

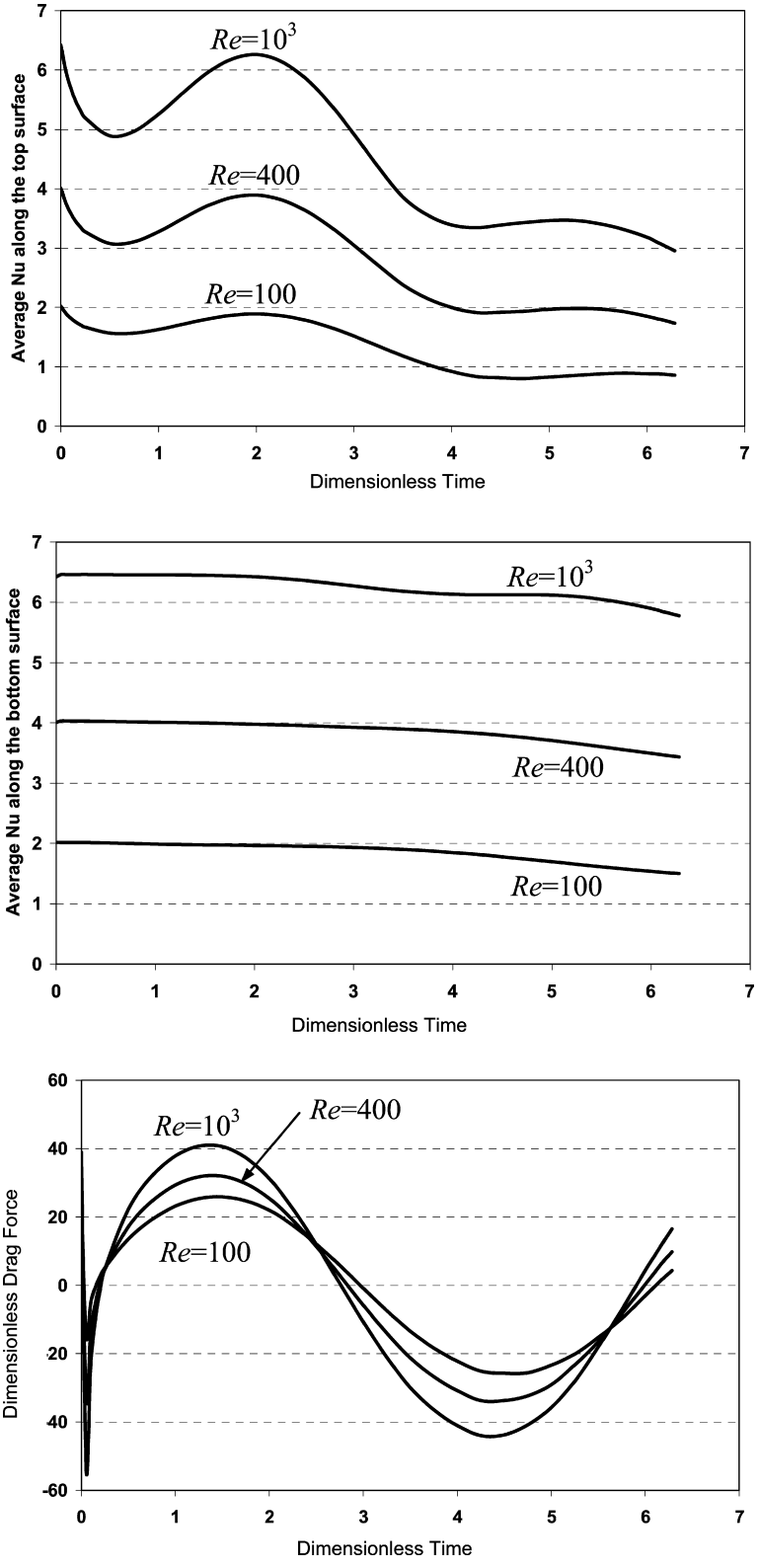

Fig. 6. Variation of the average Nusselt number and drag force predictions for $Gr = 100$ and $\varpi = 1$.

5.4. Effect of Grashof number on the temporal variation of the streamlines and isotherms

Next, the sensitivity of the streamline and isotherm patterns due to the variation in Grashof number is presented in Fig. 7 for $Re = 100$ and $\varpi = 1$. As the Grashof number increases, the intensity of convection intensifies within the cavity due to the increase in buoyancy effect. This is evident from the substantial increase in the flow circulation within the cavity at different times. For instance, at $\tau = \pi/2$: the maximum absolute circulation strength is registered at only $\Psi = 0.0893$ for $Gr = 10^3$ when compared to $\Psi = 0.128$ for $Gr = 10^4$. The Grashof number aids the flow circulation in the positive velocity cycle while it counteracts the shear effect in the negative velocity cycle. This is demonstrated through Fig. 7(a) from the existence of a secondary vortex at the lower right corner of the bottom wall for negative lid oscillating conditions. The secondary vortex is clearly visible at the maximum negative oscillating speed (i.e., $\tau = 1.5\pi$) for such a relatively small Reynolds number value. Moreover, the computed isotherms are qualitatively similar to the steady-state solution of mixed convection driven-cavity flows under positive oscillating speed conditions.

For negative speeds, however, the effect of the oscillating lid counteracts the effect of natural convection, which hinders the heat transfer activities and constrains it primarily to the conduction regime. As the Grashof number increases to 10^5, the primary vortex cell breaks up into smaller vortices as a result of a high buoyancy effect offered which overwhelms the effect of negative oscillating speed as shown in Fig. 7(b). In addition, the isotherms patterns plotted for negative oscillating speeds signals appreciated elevation in the convection heat transfer contribution to the overall heat transfer rate, as compared to $Gr = 10^3$.

5.5. Effect of Grashof number on the average Nusselt number and drag force

The effect of Grashof number on the temporal variations of the average Nusselt number and drag force is depicted in Fig. 8 for $Re = 100$ and $\varpi = 1$. This figure highlights the effect of the initial solution on the results prior to the steady periodic condition. As the Grashof number increases, the convection activities within the cavity intensify and, as a result, the average Nusselt number increases along both the top and bottom walls. This reveals that the mechanically induced lid effect is dominated by the natural convection within the cavity. The natural convection strength to that of forced convection is typically measured through the Richardson number (Ri), which is equal to Gr/Re^2. Apparently, Ri value is greater than unity for $Gr = 10^5$, which reflects buoyancy effect domination. Fig. 8 also shows that the drag force acting on the oscillating lid decreases with the increase in Gr values due to the high intensity of natural convection over the shear effect.

5.6. Effect of dimensionless lid frequency temporal variation of streamlines, isotherms, average Nusselt number, and drag force

The current investigation is wrapped by examining the implications of varying the dimensionless lid oscillation frequency (ϖ). Figs. 9 and 10 display such implications for $Re = 10^3$ and $Gr = 10^5$. It should be pointed out that the time periods outlined in Fig. 9 corresponds to the variation in the ϖ values being employed. Fig. 9(a), which presents the results for $\varpi = 0.1$, implies that the incorporation of a relatively low ϖ value facilitates the prevalence of the shear effect over the buoyancy. This will consequently permits further downward lid associated flow penetration into the cavity at the expense of the buoyancy-generated motion. Such a scenario is reversed when $\varpi = 5$ as shown in Fig. 9(b). The buoyancy effect becomes more pronounced, as it seems to limit the shear force effectiveness to a narrow distance from the sliding lid. Apparently, the increase in ϖ shortens the lid motion downward effect over the fluid. Finally, the effect of ϖ on the predicted average Nusselt number and drag force are presented in Fig. 10. This figure illustrates how quickly the steady periodic solution is reached for various ϖ. The steady periodic solution reaches quicker for large ϖ as depicted in Fig. 10. For the case of $\varpi = 5$, only the first 20 cycles are shown for simplicity. However, for a small frequency, more cycles are required to reach a steady periodic solution as demonstrated in Fig. 10. It is interesting to note that when the normalized frequency is relatively small, as seen in Fig. 10, the lid motion appreciably affects the bulk of the interior fluid. The augmentation of convective heat transfer is apparent at this condition. As the frequency value increases, the excitation of the fluid motion offered by the sliding lid becomes confined to a shallower depth of fluid. This causes the fluid to become substantially motionless in the bulk of the interior region. Therefore, the heat transfer process becomes rather ineffective in this situation. This is clearly reflected on the magnitude of the predicted

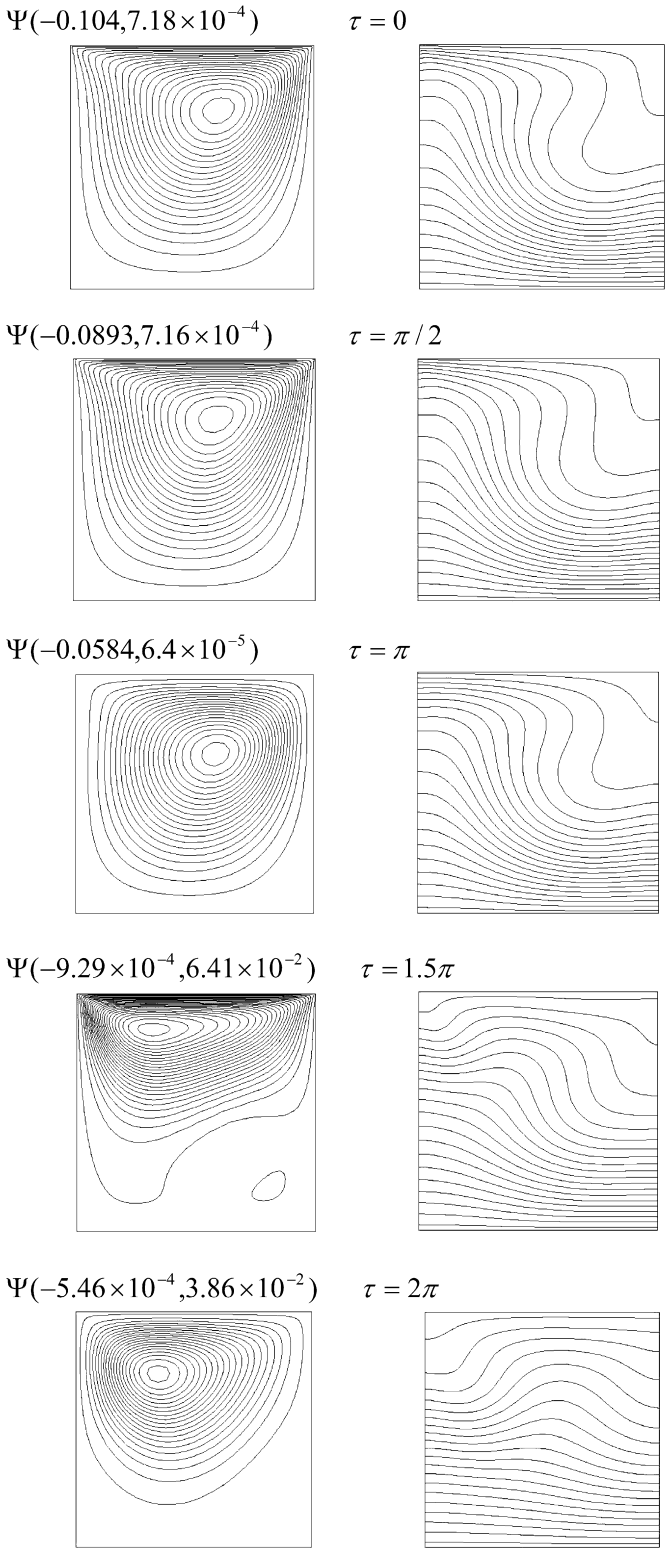

(a)

Fig. 7. (a) Variation of the streamline and isotherm contours for $Re = 100$, $Gr = 10^3$ and $\varpi = 1$. (b) Variation of the streamline and isotherm contours for $Re = 100$, $Gr = 10^4$ and $\varpi = 1$.

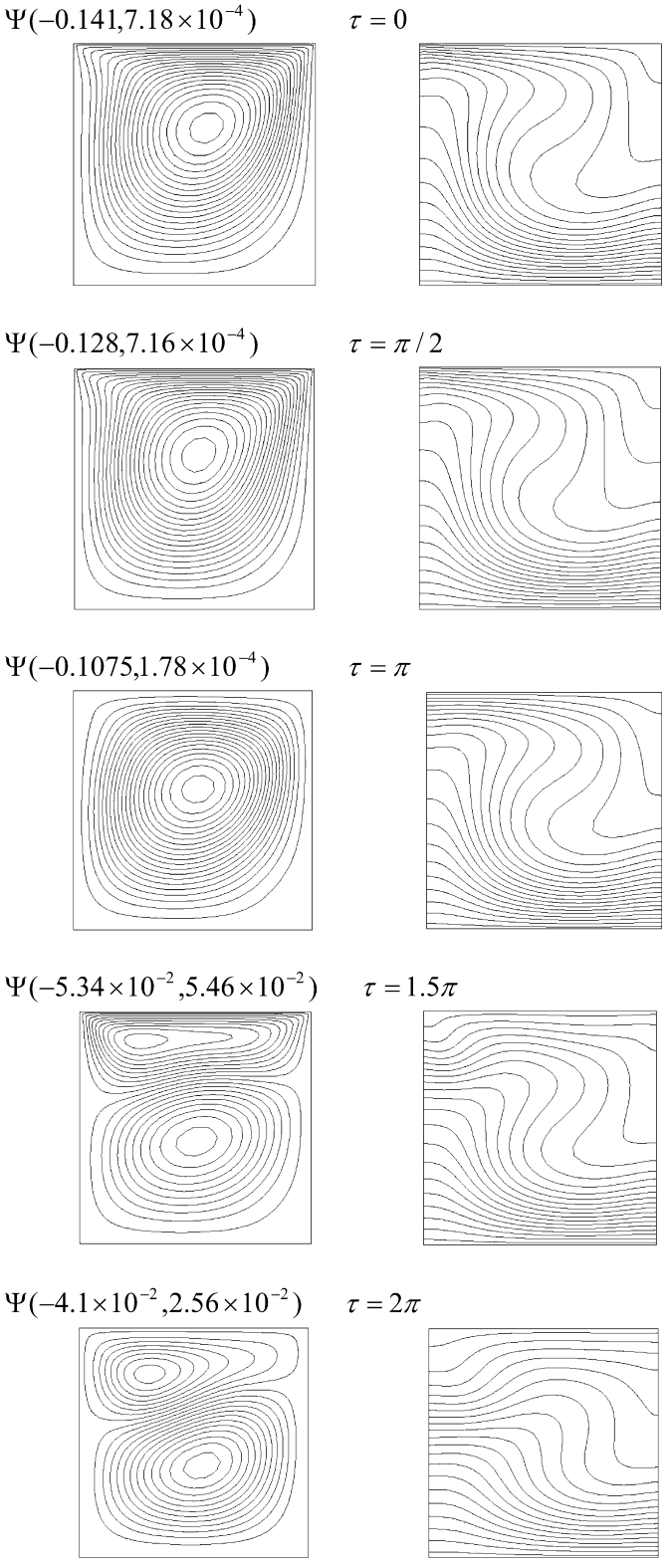

(b)

Fig. 7 (*continued*).

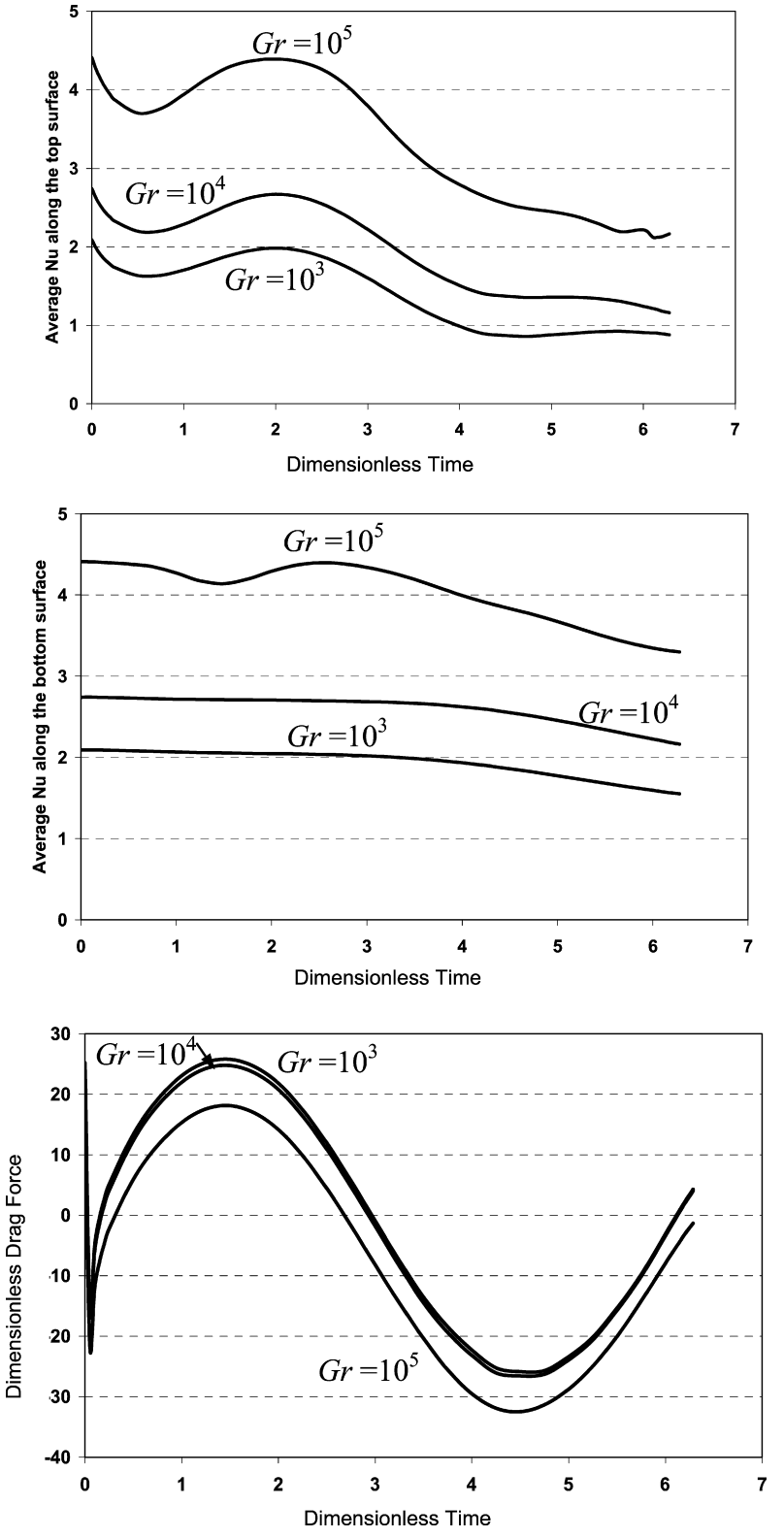

Fig. 8. Variation of the average Nusselt number and drag force predictions for $Re = 100$ and $\varpi = 1$.

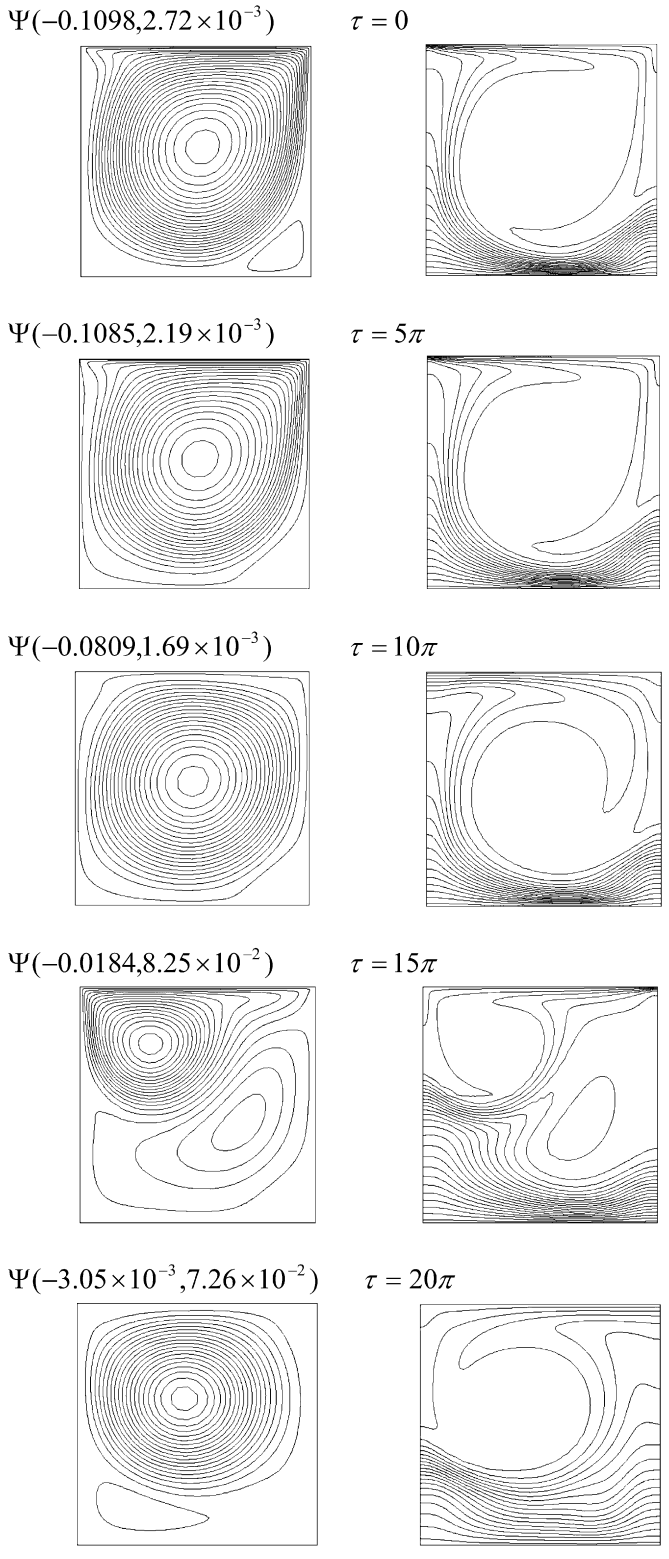

(a)

Fig. 9. (a) Variation of the streamline and isotherm contours for $Re = 10^3$, $Gr = 10^5$ and $\varpi = 0.1$. (b) Variation of the streamline and isotherm contours for $Re = 10^3$, $Gr = 10^5$ and $\varpi = 5$.

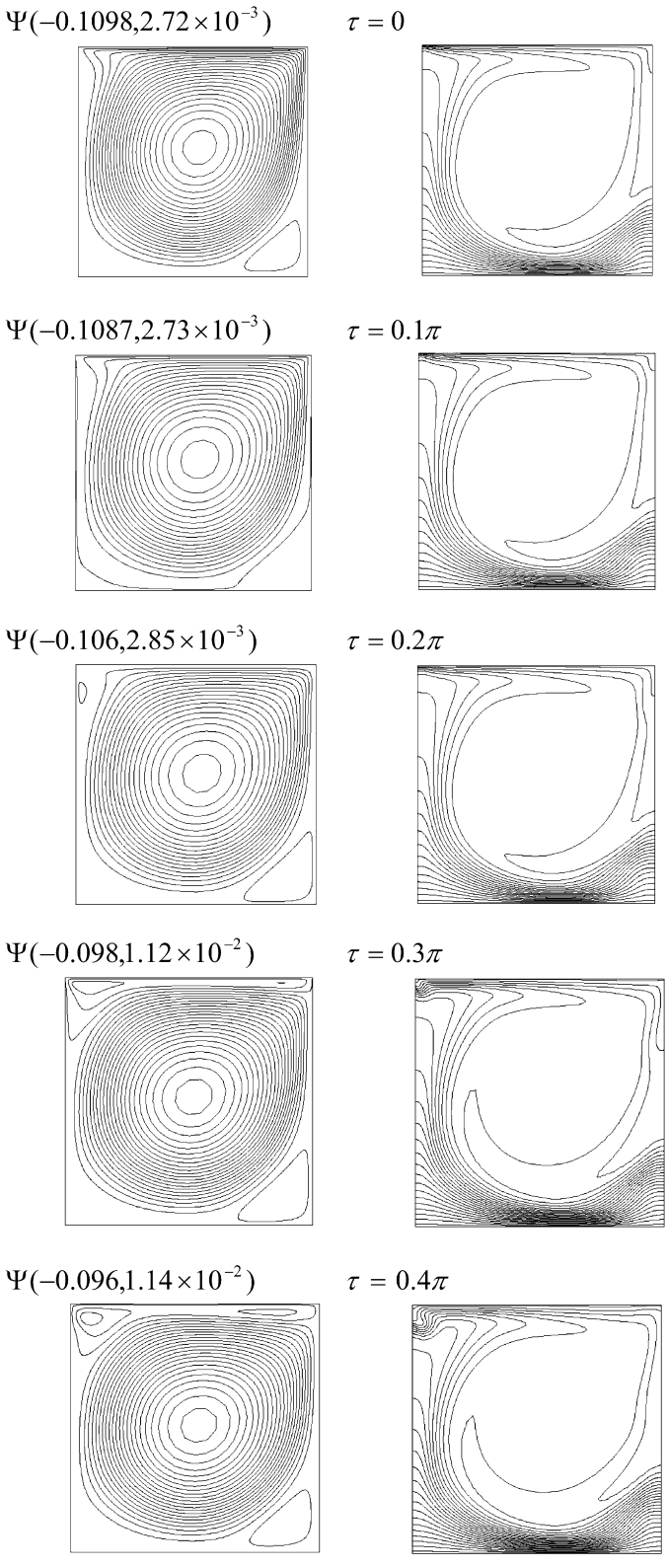

(b)

Fig. 9 (*continued*).

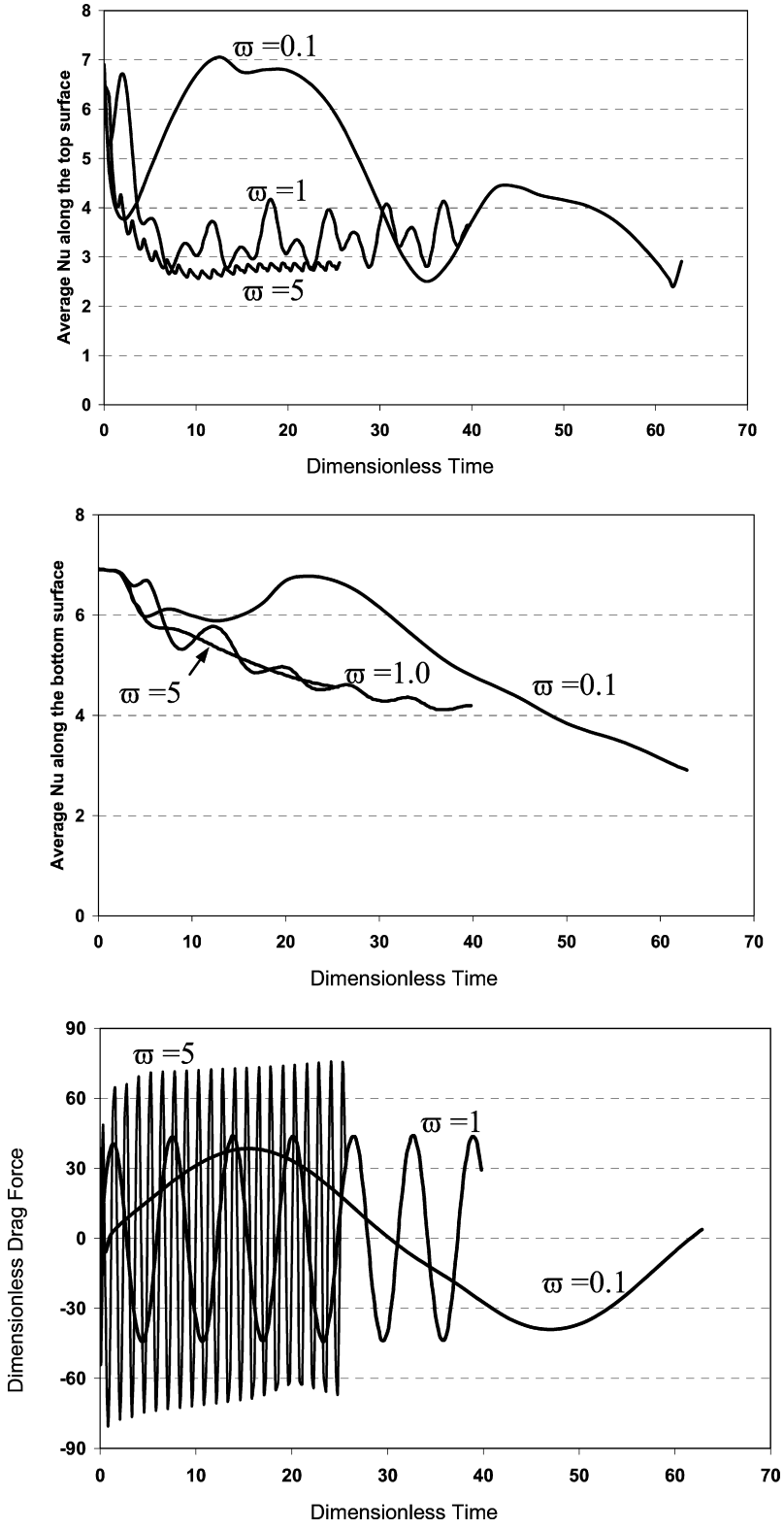

Fig. 10. Variation of the average Nusselt number and drag force predictions for $Re = 10^3$ and $Gr = 10^5$.

Nusselt numbers. Fig. 10 also demonstrates the temporal variation of the drag force at three different dimensionless lid frequencies. The results show that an elevation in the frequency value brings about an increase in the magnitude of the drag force. Furthermore, it is noticed that the drag force follows a sinusoidal oscillation pattern for moderate and high frequencies with a small deviation depicted from the external excitation sinusoidal function for the lowest frequency value considered.

6. Conclusion

Unsteady mixed convection heat transfer in a square driven cavity operating under laminar regime has been numerically investigated. An external excitation was imposed on the lid motion. The investigation was carried out for a number of pertinent dimensionless groups, namely the Reynolds number, Grashof number, and the dimensionless oscillation frequency of the sliding lid. The presented results captured the steady-periodic solutions. Such results show that the Reynolds number and Grashof number have a profound effect on the structure of fluid flow and heat transfer fields. As a matter of fact, their effects are associated with the direction of the sliding lid. Moreover, the results indicate that drag force imposed on the sliding lid increases with an increase in the Reynolds number and the lid frequency while decreases as the Grashof number increases. On the contrary, the average Nusselt number predictions increase with an increase in the Grashof number while decreases with an increase in Reynolds number and lid frequency. Finally, steady periodic solution is reached faster for small values of the normalized frequency.

References

[1] O.R. Burggraf, Analytical and numerical studies of structure of steady separated flows, J. Fluid Mech. 24 (1996) 113–151.
[2] F.J.K. Ideriah, Prediction of turbulent cavity flow driven by buoyancy and shear, J. Mech. Eng. Sci. 22 (1980) 287–295.
[3] C.K. Cha, Y. Jaluria, Recirculating mixed convection flow for energy extraction, Int. J. Heat Mass Transfer 27 (1984) 1801–1810.
[4] B.R. Baliga, S.V. Patankar, Elliptic systems: finite-element method II, in: Handbook of Numerical Heat Transfer, John Wiley & Sons, New York, 1988, pp. 421–461 (Chapter 11).
[5] M. Morzynski, C.O. Popiel, Laminar heat transfer in a two-dimensional cavity covered by a moving wall, Numer. Heat Transfer 12 (1988) 265–273.
[6] M.K. Moallemi, K.S. Jang, Prandtl number effects on laminar mixed convection heat transfer in a lid-driven cavity, Int. J. Heat Mass Transfer 35 (1992) 1881–1892.
[7] R. Iwatsu, J.M. Hyun, K. Kuwahara, Mixed convection in a driven cavity with a stable vertical temperature gradient, Int. J. Heat Mass Transfer 36 (1993) 1601–1608.
[8] R.K. Agarwal, A third-order-accurate upwind scheme for Navier–Stokes solutions at high Reynolds numbers, in: Proc. 19th AIAA Aerospace Sciences Meeting, AIAA-81-0112, St. Louis, MO, January, 1981.
[9] U. Ghia, K.N. Ghia, C.T. Shin, High-Re solutions for incompressible flow using Navier–Stokes equations and a multigrid method, J. Comput. Phys. 48 (1982) 387–411.
[10] R. Schreiber, H.B. Keller, Driven cavity flows by efficient numerical techniques, J. Comput. Phys. 49 (1983) 310–333.
[11] M.C. Thompson, J.H. Ferziger, An adaptive multigrid technique for the incompressible Navier–Stokes equations, J. Comput. Phys. 82 (1989) 94–121.
[12] J.R. Koseff, A.K. Prasad, The lid-driven cavity flow: a synthesis of quantitative and qualitative observations, J. Fluids Engrg. 106 (1984) 390–398.
[13] A.K. Prasad, J.R. Koseff, Combined forced and natural convection heat transfer in a deep lid-driven cavity flow, Int. J. Heat Fluid Flow 17 (1996) 460–467.
[14] W.H. Soh, J.W. Goodrich, Unsteady solution of incompressible Navier–Stokes equations, J. Comput. Phys. 79 (1988) 113–134.
[15] R. Iwatsu, J.M. Hyun, K. Kuwahara, Numerical simulation of flows driven by a torsionally oscillating lid in a square cavity, J. Fluids Engrg. 114 (1992) 143–151.
[16] R. Iwatsu, J.M. Hyun, K. Kuwahara, Convection in a differentially-heated square cavity with a torsionally-oscillating lid, Int. J. Heat Mass Transfer 35 (1992) 1069–1076.
[17] J.N. Reddy, D.K. Gartling, The Finite Element Method in Heat Transfer and Fluid Dynamics, CRC Press, 1994 (Chapter 4).
[18] C. Taylor, P. Hood, A numerical solution of the Navier–Stokes equations using finite-element technique, Computer & Fluids 1 (1973) 73–89.
[19] P.M. Gresho, R.L. Lee, R.L. Sani, On the time-dependent solution of the incompressible Navier–Stokes equations in two and three dimensions, in: Recent Adv. Numerical Methods in Fluids, Pineridge, Swansea, UK, 1980.
[20] A.M. Al-Amiri, Analysis of momentum and energy transfer in a lid-driven cavity filled with a porous medium, Int. J. Heat Mass Transfer 43 (2000) 3513–3527.
[21] A.M. Al-Amiri, K. Khanafer, Unsteady solution of mixed convection flow in a torsionally-oscillating square enclosure heated from below, in: Proc. 3rd Int. Conf. on Computational Heat and Mass Transfer, Banff, Canada, May, 2003.